Available online at www.sciencedirect.com

ScienceDirect

Procedia Manufacturing 47 (2020) 85–92

Procedia MANUFACTURING

www.elsevier.com/locate/procedia

23rd International Conference on Material Forming (ESAFORM 2020)

A 3D Modelling Approach for Fluid Progression during Process Simulation of Wet Compression Moulding – Motivation & Approach

Christian Poppe[a,*], Fabian Albrecht[a,b], Constantin Krauß[a], Luise Kärger[a]

[a]*Karlsruhe Institute of Technology, Institute for Vehicle System Technology, Chair of Light-Weight Technology, Rintheimer-Querallee 2, 76131 Karlsruhe, Germany*

[b]*Fraunhofer Institute for Chemical Technology, Polymer Engineering Department, Joseph-von-Fraunhofer-Str. 7, 76327 Pfinztal, Germany*

* Corresponding author. Tel.: +49-721-608-45388; *E-mail address:* christian.poppe@kit.edu

Abstract

Wet compression moulding (WCM) provides large-scale production potential for continuous fibre-reinforced structural components due to simultaneous infiltration and draping during moulding (viscous draping). Due to thickness-dominated infiltration of the laminate, comparatively low cavity pressures are sufficient – a considerable economic advantage. Experimental and numerical investigations prove strong mutual dependencies between the physical mechanisms, especially between resin flow and textile forming. Understanding and suitable modelling of these occurring physical mechanisms is crucial for process development and final part design. While existing modelling approaches are suitable for infiltration of preformed fabrics within various liquid moulding technologies, such as CRTM/RTM or VARI, WCM requires a fully coupled simulation approach for resin progression and concurrent stack deformation. Thus, the key challenge is to efficiently link these two aspects in a suitable framework. First, this work demonstrates that a three-dimensional approach for fluid progression during moulding is needed to capture WCM-process boundary conditions. In this regard, a novel test bench is used to investigate the impact of infiltration on the transversal compaction behaviour of a woven fabric. Moreover, the test setup is applied to determine the in-plane permeability values of the same material corresponding to the beforehand applied compaction states. Results are verified by comparison with an existing linear test setup.
In the second part, initial steps towards a three dimensional extension of an existing 2D modelling approach are outlined. For this purpose, a macroscopic FE-based three-dimensional formulation of Darcy's law is utilized within a User-Element in ABAQUS/EXPLICIT. Essential mechanisms within the element are presented. Additional control volumes (FE/CV) are applied to ensure mass conservation. Eventually, it is demonstrated, that the simulation model can predict the average fluid pressure beneath a punch during pre-infiltrated compaction experiments. Finally, major benefits and forthcoming steps for a fully-coupled 3D modelling approach for WCM are outlined.

Keywords: Process Simulation; FE-Forming Simulation; Wet Compression Moulding (WCM); FE/CV; Mould Filling

1. Introduction

Wet compression moulding (WCM) provides high-volume production potential for continuous fibre-reinforced components. Due to simultaneous draping, infiltration and curing, low cycle times can be achieved [1,2], as Figure 1 indicates by the process step "Viscous Draping". Due to thickness-dominated infiltration of the laminate during draping, comparatively low cavity pressures are sufficient,

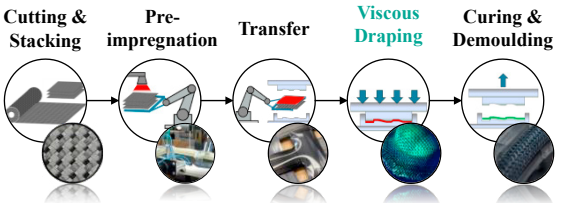

Fig. 1. WCM-Process | Process steps [3]

2351-9789
10.1016/j.promfg.2020.04.141

which makes the process economically more attractive compared to conventional liquid composite moulding processes like RTM and VARI. However, understanding and suitable modelling of occurring physical mechanisms is crucial for proper process development and final part design – in practice as well as by simulation. For the latter, WCM requires a coupled simulation approach for resin propagation and concurrent stack deformation (draping). Thus, the key challenges is to efficiently link a fluid progression model (mould filling) with an FE-Forming model, thereby considering the occurring physical interdependencies [3,4]. This implies that the occurring interactions have to be examined in advance by means of suitable experiments.

In the following, experimental results of a new test bench are presented along with a novel simulation approach, able to capture the beforehand experimentally determined interactions. One particular interesting interaction relates the current fabric deformation state and its permeability tensor $\boldsymbol{K}$. As this is also a key issue in other liquid moulding processes, a considerable number of publications addresses it, for instance within the context of CRTM/RTM [5-7] or VARI [8]. To measure permeability in fibre-reinforced composites, various techniques and methods for both characterization and evaluation of the permeability tensor are described in literature [9]. The two commonly used setups utilize a linear or radial fluid progression to determine the in-plane permeability values (K_{11}, K_{22}).

As Arbter et al. [10] pointed out, a linear setup is more likely to provide low scattering results compared to a radial setup. Yet, the linear setup is inherently susceptible to errors due to misalignment between fabric axis and flow channel. Moreover, the radial setup is recommended in cases where the principal flow axis is unknown. In either case, constant pressure or constant flow boundary conditions are applied. The resulting permeability is calculated by means of a one- or two-dimensional formulation of Darcy's law [11,12]. The latest world-wide benchmark [13] carried out by a large number of institutions, investigated unsaturated, unidirectional reinforced textiles. They demonstrate that result scattering can be significantly reduced if certain guidelines for the experimental procedures are respected.

Existing modelling approaches [8,14-16] are able to account for the above outlined interaction between deformation state and permeability tensor during infiltration within various liquid moulding technologies. However, they are not directly applicable to the WCM process, because they are not suitable for coupling with an FE-based forming simulation predicting transient large-strain deformation states. In comparison to standard fluid-structure-interaction approaches, a further challenge arises from the absence of a clear interface between fluid and deforming fabric stack, because the resin seeps through the stack during moulding. Consequently, state of the art fluid-structure-interaction codes cannot be applied in their current state.

In this work, initial steps towards a fully-coupled macroscopic 3D modelling approach for the WCM process are presented. For this purpose, an FE-based 3D formulation of Darcy's law is utilized within a User-Element in Abaqus/Explicit. The presented approach represents an expansion of an existing two-dimensional model [4]. The element is designed in a way that it can subsequently be superimposed to a suitable forming framework. By this means, a direct coupling between compaction and permeability in the textile material is enabled. Mass conservation is ensured by means of additional control volumes (FE/CV) as suggested by Trochu et al. [16].

In the following, first experimental results (Section 2) are presented, followed by the numerical modelling approach (Section 3). Finally, the prediction accuracy of the new element is exemplarily demonstrated by comparison with the presented experimental results.

2. Experimental part

In the first part of this work, the dry and pre-infiltrated transversal compaction behaviour of a 12K carbon fibre woven fabric (T700SC-12K-50C ZOLTEK fibres) is presented. Furthermore, corresponding in-plane permeability values are measured using a novel test device.

Nomenclature – Experimental part

ϕ	Fibre volume content (FVC)	[-]
n_L	Number of layers in stack	[-]
h_C	Current cavity height	[mm]
A_Ref	Reference area	[mm²]
A_Punch	Punch area	[mm²]
p_in	Inlet pressure	[MPa]
V_C	Cavity volume	[mm³]
V_F	Fibre volume in cavity	[mm³]
$\dot{V}_\mathrm{in}$	Inlet flow rate	[mm³/s]
l_i	Evaluated flow distance	[mm]
$m_\mathrm{F,A}$	Areal weight	[g/mm²]
ρ_F	Fibre density	[g/mm³]
η	Fluid viscosity	[MPas]
φ	Porosity	[-]
$\bar{v}_\mathrm{m}$	Macroscopic fluid velocity	[mm²/s]
∇p	Pressure gradient	[MPa/mm]
$\boldsymbol{K}$	Permeability tensor	[mm²]

2.1. Compaction

Compaction behaviour is analysed using a simple punch-to-plate setup mounted on a universal testing machine as shown in Figure 2. An undeformed stack of four plies is compacted with a constant punch speed of 5 mm/s. In addition to dry fabric stacks, pre-impregnated stacks are investigated using a predefined amount of silicon oil with a constant viscosity of 20 mPas. Each measurement is conducted 3 times.

The fibre volume content (FVC) ϕ is calculated using the number of layers n_L within the cavity, the areal weight of the fabric $m_\mathrm{F,A} = 0.0318\ \mathrm{g/cm^2}$, the fibre density ρ_Fibre and the current cavity height h_C according to

$$\phi = \frac{V_\mathrm{F}}{V_\mathrm{C}} = \frac{\frac{A_\mathrm{Ref} \cdot m_\mathrm{F,A}}{\rho_\mathrm{F}}}{A_\mathrm{Ref} \cdot h_\mathrm{C}} = \frac{m_\mathrm{F,A} \cdot n_\mathrm{L}}{\rho_\mathrm{F} \cdot h_\mathrm{C}} . \quad (1)$$

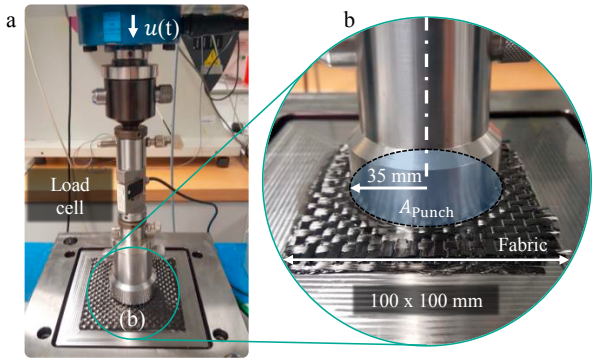

Fig. 2. Compaction | (a) Experimental device, (b) Detail view

The recorded reaction forces during compaction are plotted in Figure 3. The dry compaction curve provides a well-known non-linear shape, increasing with FVC as for instance reported by Bickerton et al. [7].

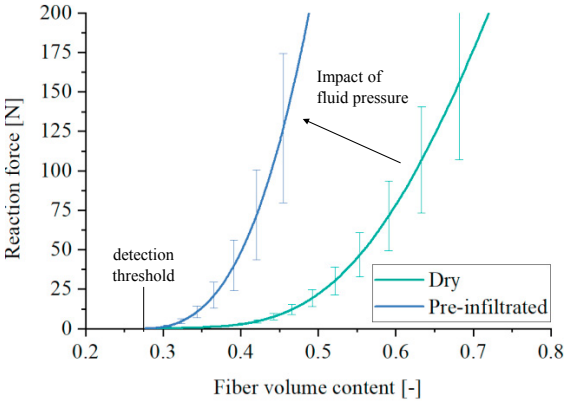

Fig. 3. Compaction | Experimental result, dry and pre-infiltrated compaction

The same principal response is obtained for the pre-infiltrated (wet) specimens. Yet, the additional occurring fluid pressure superimposes with the dry material response, resulting in a shift of the total measured reaction force towards lower FVCs. Thus, taking into account the superimposed fluid pressures during WCM process simulations will significantly alter the local compaction behaviour of the stack and thereby the predicted FVC for the final part.

2.2. Permeability

The measured superimposed fluid pressure occurs because the fluid is pushed through the porous fibre network provided by the specimens. This is commonly described using Darcy's law:

$$\bar{v}_{\mathrm{m}} = \frac{\boldsymbol{K}(\phi)}{\eta\,\varphi}\nabla p. \tag{2}$$

The macroscopic fluid velocity $\bar{v}_m$ is determined by the Permeability tensor $\boldsymbol{K}$ and porosity φ of the porous network, as well as the kinematic fluid viscosity η and the current pressure gradient ∇p. Darcy's law is further used to determine the permeability values of a porous network by applying either a constant pressure boundary condition and measure the resulting fluid flow rates (progression) or vice versa.

In this work, a novel test bench as illustrated in Figure 4 is utilized, where the fabric is positioned between two plates of a mould. The upper plate is designed to provide a circumferential clamping area of constant width. A video extensometer is used to minimize the uncertainties of the mould cavity, especially for increased FVCs.

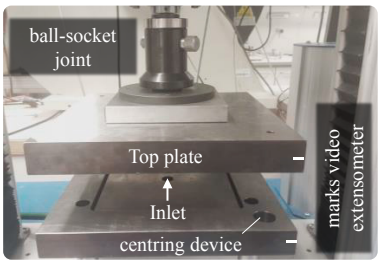

Fig. 4. Permeability | Experimental device

A one-dimensional flow across the clamped area is assumed for the evaluation of test results (see Figure 5). To conduct the trial, first a target gap (target FVC) is accessed, and then a test fluid is injected using a constant volume flow. When the cavity pressure has reached a stationary state, a value is recorded. A ball-socket joint is applied to the top plate in order to ensure a homogeneous distribution of the compaction forces.

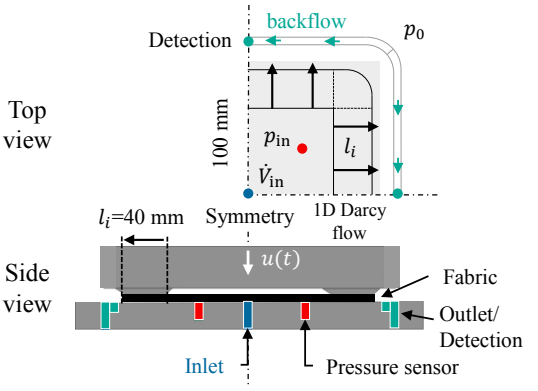

Fig. 5. Permeability | Schematic illustration of the measuring principle

As shown in Figure 5, the backflow at each side is detected and taken into account during the calculation of the permeability values. Each measurement is conducted 3 times with fresh material.

Although this setup is rather complex, it provides certain advantages. First, any formation of flow channels between fabric and wall is prevented, similar to a radial setup. Furthermore, the modular top plate enables to modify the clamping area geometries. By this, FVCs up to 80 % can be reached with a normal tensile testing machine (50 kN). This high compaction states are important to investigate because they can occur in sealing areas during the WCM process and are therefore vital for an accurate prediction of the cavity

pressure. Moreover, sheared fabric specimens can be evaluated without further adaption of the test setup.

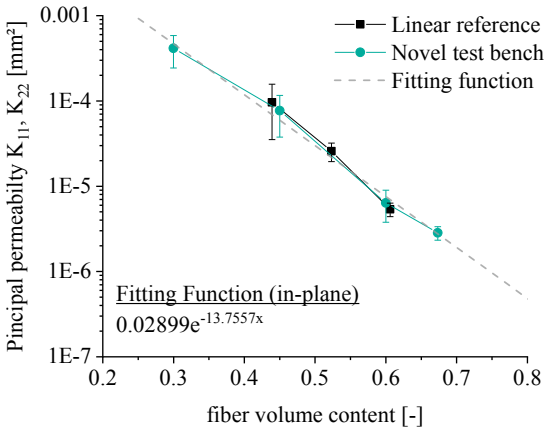

Fig. 6. Permeability | Results

The presented setup is used to determine the principal permeability values (see Figure 6, green marks) for different compaction states of a four-ply stack of a balanced woven fabric, which was not subjected to any in-plane shear deformation. Compaction of the material significantly increases the flow resistance. Values ranges and tendencies are in agreement with existing literature [9,12,14] for comparable materials. To validate the presented test setup, the obtained permeability values are compared with previous tests (see Figure 6, black marks), which were conducted with a linear setup as presented by Magagnato et al. [6] for the same material. The good agreement demonstrates the reliability of the presented test bench.

3. Numerical part

Nomenclature – Numerical part

N	Nodal index $N = \{1 \dots 6\}$	[-]
I	Surface index $I = \{1 \dots 5\}$	[-]
X_k^N	Current coords. of node N of el. k	[mm]
p_k^N	Pressure at node N of element k	[MPa]
$\dot{V}_k^I$	Flow rate at Surface I of element k	[mm³/s]
$\boldsymbol{K}$	Permeability tensor	[mm²]
K_{11}	Permeability in warp direction	[mm²]
K_{22}	Permeability in weft direction	[mm²]
ϕ_k	Fibre-volume-content	[-]
V_k	Element volume	[mm³]
V_k^{free}	Free volume	[mm³]
V_k^{fluid}	Fluid volume	[mm³]
V_k^{fibre}	Fibre volume	[mm³]
S_k	Saturation	[-]
$u(t)$	Displacement profile	[mm]
μ	Porosity	[-]
η	Fluid viscosity	[MPas]

Literature review along with the above outlined experimental results prove that key mutual physics-based dependencies within the WCM process cannot be properly accounted for without a three-dimensional simulation approach, similar to insights regrading process simulation approaches in other liquid moulding processes (e.g. VARI). In the following, a macroscopic FE-based three-dimensional formulation of Darcy's law is utilized within a User-Element (VUEL) in ABAQUS/EXPLICIT.

3.1. Darcy Progression Element (DPE3D)

Given the objective, that the new element shall be superimposed to a structured FE-Forming mesh in forthcoming analyses, a wedge-shape element as illustrated in Figure 7 is selected. The element consist of six nodes and five surfaces over which the pressure corresponding surface flows are to be evaluated.

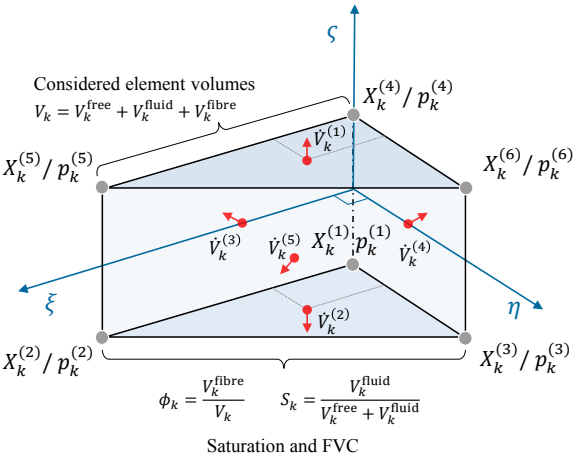

Fig. 7. Isoparametric element formulation with pressures p_k^N at node N and surface flows $\dot{V}_k^I$ at surface I of element k within the current configuration

In every element k, the total volume V_k comprises certain amounts of fibre V_k^{fibre}, fluid V_k^{fluid} or free V_k^{free} volume. Fibre volume content and element saturations are updated accordingly in every increment. Since every node contains a pressure degree of freedom (DoF), pressure gradients in thickness direction are captured by the three-dimensional formulation. Gaussian integration scheme in conjunction with six integration points is applied. Six integration points are required in order to accurately calculate the conduction matrix within the element during large strains in combination with perchance-high element aspect rations (10-25).

The following key mechanisms are to be implemented within the new DPE3D element:

- Solution of the pressure field within the saturated domain
- Progression of the resin front and mass conservation
- Modification of the pressure due to compaction

Saturated elements ($S_k = 1$) are part of a saturated domain on which the system equation is solved, whereas a global algorithm based on an additional control volume (CV) additionally treats empty and filling elements. To improve clarity, the Element index k for the Elements is omitted.

Saturated domain

Regarding the saturated domain, Richard's law [12] is applied, which provides the combination of mass conservation and Darcy's law. Hence, mass conservation is achieved when the overall flow rate $\dot{V}$ within the saturated domain equals zero

$$\dot{V} = \int_V \operatorname{div}\left(\operatorname{grad}\left(\frac{\boldsymbol{K}(\phi)}{\varphi\,\eta} p\right)\right) \mathrm{d}v \to 0\,. \tag{3}$$

In addition to displacements and rotations, user-defined finite elements in ABAQUS/EXPLICIT provides a temperature as well as a pressure nodal degree of freedom (DoF). Both can be utilized within a fully coupled structural-thermal analysis to model forming and fluid progression simultaneously. As presented in [4], the analogy between the equation of heat conduction (Fourier's Law) and Richard's law can be used to formulate an explicit transient formulation of Equation 3. By this means, fluid progression can be accounted for by introducing a nodal hydraulic capacity C_{hd}^{N} along with a linear isoparametic formulation for the wedge-shape element

$$\underline{\underline{M}}^{\mathrm{mass}}\ \dot{\underline{p}} = \underline{\underline{M}}^{\mathrm{cond}}\ \underline{p} + \underline{S}^{\mathrm{comp}}\ . \tag{4}$$

Here, mass matrix $\underline{\underline{M}}^{\mathrm{mass}}$ contains the nodal hydraulic capacities C_{hd}^{N} , which should be as small as numerically feasible to represent a quasi-incompressible fluid, although an explicit time integration scheme is applied [4]. Moreover, a source vector $\underline{S}^{\mathrm{comp}}$ is added to the right-hand-side of the system equation to account for local compaction induced fluid pressures.

$$\underline{\underline{M}}^{\mathrm{mass}} = \rho C_{\mathrm{hd}}^{N} \underline{\underline{I}} \to 0 \tag{5}$$

The conduction matrix $\underline{\underline{M}}^{\mathrm{cond}}$ connects the element permeability tensor $\underline{\underline{K}}$ with the $\underline{\underline{B}}_1$-Matrix, which provides the spatial deviations of the linear element interpolation functions for the wedge element in its current configuration:

$$\underline{\underline{M}}^{\mathrm{cond}} = \frac{\det\left(\underline{\underline{J}}_1\right)}{\varphi\,\eta} \cdot \underline{\underline{B}}_1 \cdot \left(\underline{\underline{K}}(\phi)\right) \cdot \underline{\underline{B}}_1^{\mathrm{T}}\,. \tag{6}$$

The determinant of the Jacobian matrix accounts for a potential change of element volume.

Flow front progression & mass conservation

Beyond the determination of the pressure distribution within the saturated domain, a physical based implementation of the flow front progression is needed to ensure mass conservation. Therefore, a transient global control volume (CV) is implemented including all elements that contain fluid volume. Similar to [4], the two tasks of the global CV are the determination of the accumulated propagated flow at the flow front and its partition on the filling elements. The deformed configuration is used to calculate the incremental surface flows $\dot{V}^I$ based on the normal vectors $\underline{n}^I$ of the surfaces $I = \{1 \dots 5\}$ within every element (cf. Figure 7).

$$\dot{V}^I = \det\left(\underline{\underline{J}}_1\right) \Delta t_{\mathrm{inc}} \left(\frac{\underline{\underline{K}}(\phi)}{\varphi\,\eta} \cdot \underline{\underline{B}}_1^{\mathrm{T}} \cdot \underline{\underline{J}}_1^{-\mathrm{T}} \cdot \underline{p}\right) \cdot \underline{n}^I \tag{7}$$

The summed incremental volume flow of every element has to be zero for an incompressible fluid. Hence, mass conservation within every element is implied if the surfaces flows are being calculated correctly. This is checked by the elements during the analysis. Since Richard's law is applied for the system equation, mass loss within the saturated domain is prevented. For FE-based formulations, this can still be an issue at discrete element surfaces within the saturated domain as demonstrated by Josh et. al. [17]. Therefore, the outer edges of the global CV, including the flow front edges, are used for a second mass conservation check within the model. The individual contribution of the elements to the global CV depends on their state (empty, filling or saturated) and their location (inlet, vent, wall or flow front). The latter is also utilized to account for process boundary conditions. Prior numerical study proved that, by tracing the mass loss within elements and the whole model, mass conservation could be achieved with an accuracy of 99.5 % during large deformations.

Further, an algorithm based on the pressure gradient and the area of the filling elements is implemented to determine the partition of the summed propagation flow. By this means, a mesh-independent flow front progression is achieved [4]. The saturation S within the filling elements is updated accordingly until their saturation reaches one (see Fig. 7). This workflow is repeated incrementally within the analysis.

Modification of the saturated domain pressure

Finally, the third essential mechanism is the local response of saturated elements to compaction. In fact, this refers to any decrease/change of the element volume V_k, whether due to compaction or exemplary shear deformation. Since any saturated element contains a certain amount of fluid volume, a local overflow is generated in all these cases. This local overflow is utilized to modify the local pressure field. Exemplary, if a certain number of elements is being compacted, all of them try to locally increase the pressure distribution of the domain until the flow at the front flow matches the compaction induced fluid displacement. This implies, that the overall flow resistance between the local overflow position and the current flow front position is accounted for intrinsically, including all local effects such as fibre orientations or deformation states.

Thus, the fluid must progress through the saturated domain and is not directly transferred to the flow front. While doing so, a slight pressure overshoot cannot be avoided completely due to the explicit integration scheme in conjunction with discrete element surfaces. However, these effects are only relevant for relatively coarse meshes that would not be in fact not suitable for process simulation anyway.

3.2. Verification – Linear flow scenario

Regarding WCM, forced infiltration due to compaction through a porous medium is the most relevant process condition. For this work, a test case inspired by Bickerton al. [7] including two phases (see Figure 8), injection (blue) and subsequent compaction (red), is selected since it enables a two-step verification of the model with increasing complexity. Whereas the injection phase (constant inlet pressure) allows verification and testing of fundamental functionalities within the element, such as implementation of the system equation, time integration scheme, flow front progression and mass conservation, the compaction phase enables to verify the overflow-based modification of the saturated domain pressure.

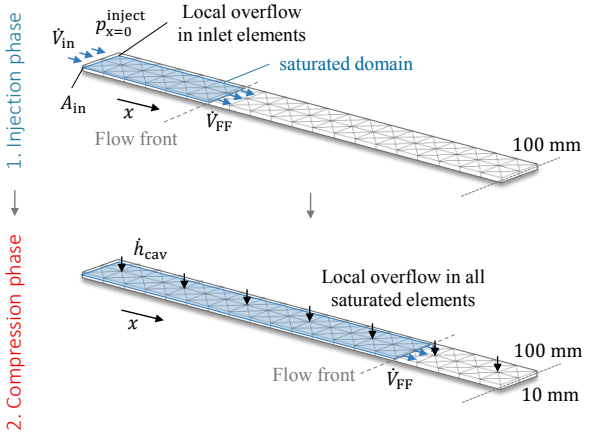

Fig. 8. Linear flow case | Boundary conditions for the injection and compression phase of the linear flow case

As illustrated in Figure 8, a strip (10 x 100 mm) containing 160 structured elements is first subjected to a constant inlet pressure $p^{\text{Inject}}_{x=0} = 1\,\text{MPa}$ and subsequently to constant compaction $\dot{h}_{\text{cav}} = 0.03\,\text{mm/s}$. During injection, at total fluid volume of $V_0^{\text{fibre}} = 134\,\text{mm}^3$ is being injected, resulting in a flow front position of 60 mm. Principal permeability $K_x(\phi_1)$ is chosen according to of the experimental results presented in Section 2.2. Thus, a constant FVC of $\phi_1 = 44\,\%$ is presented during the first phase, whereas FVC increases up to $\phi_1 = 57\,\%$ during the second phase.

The analytical solution [12] for the transient flow front $x^{\text{inject}}_{\text{FF}}(t)$ within the injection phase is given by

$$x^{\text{inject}}_{\text{FF}}(t) = \sqrt{\frac{2K_x \cdot p^{\text{inject}}_{x=0} \cdot t}{(1-\phi_1)\cdot\eta}}\,. \tag{8}$$

Regarding the compaction phase, the analytical solution for the flow front position directly follows from mass conservation of the previously injected incompressible fluid V_0^{Fluid}

$$x^{\text{comp}}_{\text{FF}}(t) = \frac{V_0^{\text{Fluid}}}{hb\cdot(1-\phi_1)}\,. \tag{9}$$

Figure 9 provides a comparison between the analytical solutions and the numerical predictions for both phases in terms of the flow front progression – a good agreement can be achieved.

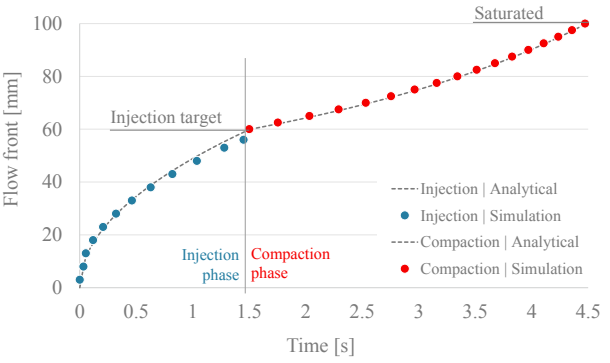

Fig. 9. Linear flow case | Comparison between analytical and numerical prediction for the flow front progression during injection and compaction

Since the flow front progression within the injection phase is intrinsically linked with the global pressure distribution within the strip, this implicitly verifies the transient pressure distribution. However, this does not apply to the compaction phase where a good consistency with the analytical solution only proves that mass conservation is achieved. As the overflow is used to manipulate the pressure distribution of the saturated domain, it might be possible to achieve comparable flow front progression with unsuitable high pressures or a false pressure distribution across the strip.

Accordingly, the transient pressure during compaction should also be verified. An analytical solution is exemplarily provided by Bickerton et. al. [7] according to

$$p^{\text{Comp}}(x) = \frac{\eta\cdot\dot{h}_{\text{cav}}}{2h_{\text{cav}}\cdot K_x(\phi_1)}\left(x^2 - x^2_{\text{FF}}\right), \tag{10}$$

where x_{FF} is current flow front progression. Figure 10 proves a good agreement between analytically and numerically predicted pressure distribution across the strip for two distinct points in time during compaction.

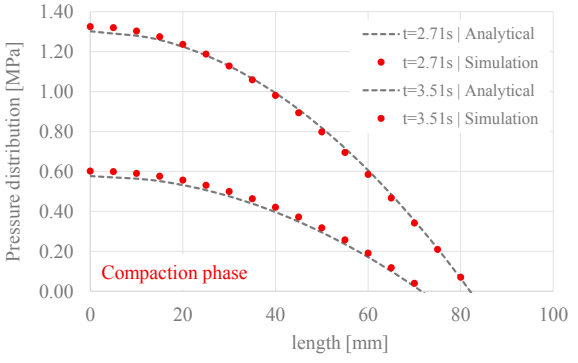

Fig. 10. Linear flow case | Comparison of the predicted pressure distributions within the specimen during compaction phase

The presented results demonstrate that the presented model is able to predict transient flow front progression and pressure distribution during both injection and compression with suitable accuracy. This implies that the introduced mechanisms of the model, such as mass conservation, time integration scheme of the system equation and overflow-based modification of the pressure distribution work properly for the demonstrated test case.

3.3. Comparison with experiments

For further investigation, the outlined modelling approach is used to simulate the pre-infiltrated compaction trials outlined in Section 2, cf. Figure 2b. Assuming, that the compaction behaviour of the woven fabric is not significantly affected by the presence of the fluid, the resulting averaged fluid pressure curve can be extracted from Figure 3 by subtracting pre-infiltrated and dry experimental curve. This difference curve represents the averaged fluid pressure beneath the punch, which is superimposed to the recorded reaction force during pre-infiltrated tests. Only a quarter of the test setup modelled within the numerical simulation because of its rotational symmetry.

Figure 11 displays a visual comparison between the experimental and numerical setup. The numerical model provides an insight into the corresponding pressure distribution below the punch.

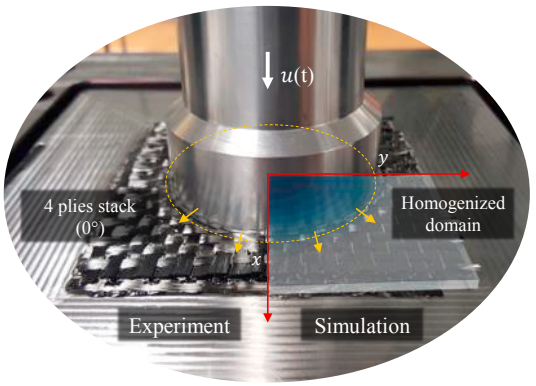

Fig. 11. Visual comparison between experimental setup and numerically predicted pressure distribution beneath the punch (blues)

In order to introduce the measured material behaviour to the model, the above presented function of the permeability (Figure 6) is implemented. By this means, the model is able to account for the significant increase of the in-plane permeability values during compaction.

For simplification, the four-ply stack is homogenized to one single layer within the simulation setup. As all four plies provide the same fibre orientations (0/90°), a simple adjustment of the experimentally determined areal weight $(4 \cdot m_{\mathrm{F,A}})$ is sufficient. Moreover, an impact of gravity is neglected as well as any fluid-structure-interaction between fabric and fluid except for the homogenized flow resistance captured within Darcy's Law.

Regarding boundary conditions within the simulation, the required amount of fluid volume is applied via predefined saturation values of corresponding elements. Furthermore, compaction is implemented by means of a displacement boundary condition for the punch, which is modelled using a discrete rigid elements. A constant closing speed of 5 mm/min. is applied according to the experimental tests. As shown in Figure 12, the average fluid pressure beneath the punch area is well predicted by the simulation. Significant deviations only occur towards the end of compaction.

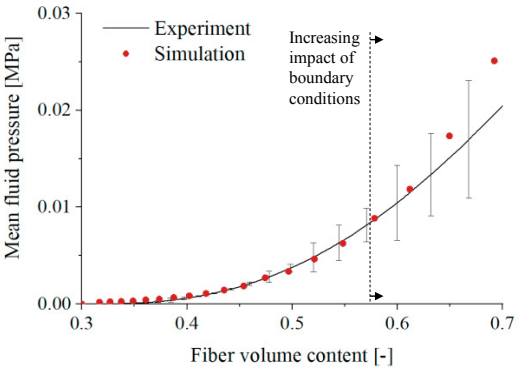

Fig. 12. Comparison between experimental determined and numerically predicted average fluid pressure beneath the punch

This deviation is reasonable, since the flow front is located outside the punch area towards the end of compaction. From this point onwards, the boundary conditions between experiment and numerical model deviate. Whereas the fluid within the numerical model still progresses through a porous medium, this assumption is not valid anymore in experiments. Nonetheless, during a large part of the compaction phase, the flow front is located within the punch radius and the presented model is able to predict the experimentally determined pressure beneath the punch correctly, despite the introduced simplifications.

4. Discussion & Conclusion

Dry and pre-infiltrated compaction behaviour of a woven fabric is measured experimentally using a new test bench. The results demonstrate the significance of superimposed fluid pressure and its effect on the resulting compaction force. The qualitative results are in good agreement with the findings of Bickerton et al. [7] Since the same interdependencies occur in wet compression moulding (WCM), numerical process simulation tools should be able to capture them in order to support design and process development.

Moreover, a new test bench is used to determine the in-plane permeability values (K_{11}, K_{22}) corresponding to the priorly investigated compactions states. The results are in agreement with existing literature for comparable materials [10,12,13]. Furthermore, the validity of the new test setup is demonstrated by comparison with linear flow tests conducted with the same material [6]. The experimental results are used to identify a functional relation between permeability and fibre-volume-content, which is embedded in the numerical model.

The presented experimental results along with existing literature [1-3] prove that a suitable process simulation

approach for WCM must capture concurrently a three-dimensional fluid progression during moulding. Beyond that, the model should be able to capture the relevant process boundary conditions, for example initial resin distribution, curing state, tool geometries, tool temperature and not to mention a suitable draping model including compaction and corresponding fibre-frame dependent permeability values. Although, the initially published two-dimensional approach [4] enables a simultaneous fluid progression under consideration of local deformations and fibre orientations during moulding, it disregards any effects in thickness direction such as compaction.

To overcome this, a three-dimensional extension of this initial 2D modelling approach is presented in this work. A macroscopic FE-based formulation of Darcy's law is utilized by means of a User-Element in ABAQUS/EXPLICIT. Furthermore, three essential mechanisms are outlined and described. The first mechanism (Section 3.1.1) account for the pressure distribution within saturated domain under consideration of arbitrary, large deformation states, local fibre orientation and potentially high aspect ratios. The second mechanism (Section 3.1.2) enables flow front progression and ensures mass conservation via an additional control volume. The last mechanism (Section 3.1.3) allows for a local overflow dependent modification of the pressure distribution within the saturated domain.

A linear flow test case is applied to verify the models response to both injection and compression via analytical solutions. For the considered test case, the new model is capable to predict the flow front progression and pressure distribution during injection and compaction correctly. Moreover, comparison with experimental result are encouraging as the model is able to predict average fluid pressure during compaction, even though the presented approach neglects free surface and multiphase flows in its current state.

The numerical prediction of injection and forced infiltration phenomena utilized either by Stokes's law, Darcy's law, or even a combination of them, have been subject to several studies within the last 30 years [8,12,15-17]. Thus, the presented numerical results in this study are no completely novel. However, proving functionality of the presented fluid model marks only the first important step. In the future, the presented approach will provide the possibility to account for fluid propagation under large strains during forming in a numerically efficient and monolithic manner. Due to its explicit formulation, the presented model can simply be superimposed to existing forming simulation models by adjusting the permeability functions embedded in the fluid model.

Thus, future work will focus on the expansion of the presented approach to multilayer laminates, including interface fluid exchange, a proper fluid-structure-interaction (FSI) between fluid pressure and stack deformation, suitable representation of the mould cavity as well as curing. For this purpose, a suitable forming framework is required, which must enable local compaction in thickness direction. This is already a very important and ongoing issue in the field of FE forming simulation. An effective combination of a suitable forming framework and the presented new DPE3D element will enable the prediction of cavity pressures, local FVC, fibre orientations and impregnation behaviour by taking into account the physics-based interdependencies during WCM-processes.

Acknowledgements

The authors would like to thank the German State Ministry for Science, Research and Art of Baden-Württemberg (MWK) for the funding of the project "Forschungsbrücke Karlsruhe-Stuttgart" for which the presented work is carried out. The work is part of the Young Investigator Group (YIG) "Tailored Composite Materials for Lightweight Vehicles", generously funded by the Vector Stiftung.

References

[1] Bergmann J, Dörmann H, Lange R. Interpreting process data of wet pressing process. Part 2: Verification with real values. Journal of composite materials 2016;50:2399-2407

[2] Bockelmann P. Process Control in Compression Molding of Composites, doctoral thesis. Fakultät für Maschinenwesen. Technical University Munich 2017

[3] Poppe C, Rosenkranz T, Dörr D, Kärger L. Comparative experimental and numerical analysis of bending behaviour of dry and low viscous infiltrated woven fabrics. Composite Part A 2019;124:105466

[4] Poppe C, Dörr D, Henning F, Kärger L. A 2D modeling approach for fluid propagation during FE-forming simulation of continuously reinforced composites in wet compression moulding. AIP Conference Proceedings 2018:020022

[5] Chen B, Lang E, Chou, TW. Experimental and theoretical studies of fabric compaction behavior in resin transfer molding. Materials Science and Engineering 2001;317:188–196

[6] Magagnato D, Thoma B, Henning F. Experimental characterization to determine the influence of different binder systems on the preform permeability during RTM manufacturing. Journal of Plastics Technology 2015:1864-2217

[7] Bickerton S, Abdullah MZ. Modeling and evaluation of the filling stage of injection/compression moulding. Composites Science and Technology 2003;63:1359–1375

[8] Dereims A, Drapier S, Bergheau J, de Luca P. 3D robust iterative coupling of Stokes, Darcy and solid mechanics for low permeability media undergoing finite strains. Finite Elements in Analysis and Design 2015:94,1-15

[9] Sharma S, Siginer D. Permeability Measurement Methods in Porous Media of Fiber Reinforced Composites. Applied Mechanics Reviews 2010;1-19

[10] Arbter R, Beraud JM, Binetruy C, Bizet L, Bréard J, et al. Experimental determination of the permeability of textiles: A benchmark exercise. Composites Part A 2011;42:1157–1168

[11] Darcy H. The Public Fountains of the City of Dijon. Dalmont 1856. Paris

[12] Rudd CD, Long AC, Kendall KN, Mangin C. Resin Transfer Moulding-Structural Reaction Injection Moulding and Related Processing Techniques, Woodhead Publishing 1997, ISBN 978-1-84569-544-6

[13] Vernet N, Ruiz E, Advani S, et al. Experimental determination of the permeability of engineering textiles: Benchmark II. Composites Part A 2014;61:172–184

[14] Veronique M. A Review of Non-saturated Resin Flow in Liquid Composite Moulding processes. Transport in Porous Media 2016;115:581-601

[15] Buschke M, Advani S. A Finite Element/Control Volume Approach to Mold Filling in Anisotropic Porous Media, Polymer Composites 1990;11: 398-405

[16] Trochu F, Gauvin R, Gao D. Numerical Analysis of the Resin Transfer Molding Process by the Finite Element Method, Advances in Polymer Technology 1993;12:329-342

[17] Joshi SC, Lam YC, Liu XL. Mass conservation in numerical simulation of resin flow. Composites Part A 2000;31:1061-1068